

Zonal Flows and Fields Generated by Turbulence in CHS

A. Fujisawa, K. Itoh, A. Shimizu, H. Nakano, S. Ohshima, K. Matsuoka, S. Okamura,
CHS-group

National Institute for Fusion Science, Oroshi-cho, Toki, Japan 509-5292

The paper reports two major progresses made in heavy ion beam probe (HIBP) measurements carried out in CHS. One is to prove the nonlinear couplings between zonal flows and turbulence by using the modern nonlinear data analyzing techniques. The other is the identification of zonal magnetic field, generated by the turbulence, utilizing the potential ability of the HIBP. The measurements of magnetic field fluctuations successfully provide the fluctuation spectrum, and the first experimental evidence of the turbulence dynamo, which is a long-standing historical candidate for the geomagnetism and analogous phenomena, that the turbulence generates a structured magnetic field.

Keywords: zonal flows, turbulence, zonal magnetic field, heavy ion beam probe, nonlinear interaction, mesoscale structure, dynamo, wavelet bicoherence analysis

1. Introduction

Turbulence is a ubiquitous phenomenon observed in the universe. It has been recognized that the turbulence is not the process of randomization, but also the one to produce a structure. For example, it is well known that the Rossby wave turbulence should generate the Jovian belt or zonal flows [1], and that turbulence should be the cause for the geomagnetic (dipole) field. In 1970s, it was pointed out that the drift wave turbulence should obey the same equation as the Rossby wave turbulence [2], therefore, it is expected that the zonal flows should exist in toroidal plasmas.

In the research of magnetic confinement, recently, the importance of the zonal flows has been recognized since the saturation level of drift wave turbulence, which governs the transport processes, should be determined by the interaction between zonal flows and drift waves [3]. After the evidence to hint the zonal flows and their roles in transports was presented in theoretical and simulation works [4-6], the existence of zonal flows was experimentally proven in a number of devices [7-19] (for review [20]).

After the identification of the zonal flows [4], the CHS experiments have made a great progress in the physics of zonal flows and turbulence. The investigation has been made on the interaction or nonlinear coupling between zonal flows and turbulence [21-24]. Besides, we have developed a potential ability of the heavy ion beam probe (HIBP), which means the direct measurement of magnetic field fluctuations of plasma interior from the horizontal secondary beam movement, and successfully obtained a spectrum of magnetic field fluctuations in CHS

plasmas [25].

The paper presents the direct quantitative evidence to show the coupling between zonal flows and turbulence with an advanced analysis technique, the wavelet bicoherence, and presents the existence of zonal magnetic field, as well as zonal flows, with recently developed technique of the magnetic field fluctuation measurement with HIBP. The discovery of the zonal magnetic field should be the first evidence to show that the turbulence really generates the structured magnetic field, which is associated with a historical physics problem, i.e., dynamo problem.

2. Experimental Set-up

CHS is a toroidal helical device of which the major and averaged minor radii are $R=1$ m and $a=0.2$ m, respectively. The device is equipped with two HIBPs to measure plasma potential in different toroidal sections apart by 90 degree. Each HIBP has three channels to observe the adjacent spatial points of the plasma. The local electric field can be directly measured by making a difference between potentials of neighboring two channels.

It has been known for HIBPs, in addition to the electrostatic potential, that a vector potential component can be measured from the beam movement on the detector; particularly in an axisymmetric magnetic configuration, a formula is derived to relate the movement to the toroidal component of the vector potential [26]. In a real geometry, the fluctuation of a magnetic field component, or derivative of vector potential, can be directly measured by taking the

difference between the beam movements on the detectors from the neighboring ionization points. The details of the method are described in ref. [25].

3. Coupling between Zonal Flows and Turbulence

The target plasmas for the experiments introduced below are produced with electron cyclotron resonance heating of ~ 200 kW. The magnetic field strength of the discharges is $B=0.88$ T, and the density is kept constant approximately at $n_e \sim 5 \times 10^{12} \text{ cm}^{-3}$. The HIBP measurement is performed at $\rho \sim 0.35$, where the amplitude of zonal flow tends to be large, which gives a better condition to investigate the interaction between zonal flows and turbulence.

In this discharge condition, electron and ion temperatures $T_e \sim 0.5$ keV, $T_i \sim 0.1$ keV, (i.e., in collisionless regime), ion Larmor radius $\rho_i \sim 0.1$ cm, time scale of micro-instabilities $\omega^*/2\pi R \sim 50$ kHz with $k_{\text{perp}} \rho_i \sim 0.3$ and energy confinement time $\tau_E \sim 2$ ms (or characteristic frequency of global confinement $\tau_E^{-1} \sim 0.1$ kHz), where k_{perp} is the wavenumber and ω^* is the drift frequency defined as $k_{\text{perp}} T_e / eBL_n$ with L_n being a characteristic length of density gradient. Here the pressure-gradient-driven microinstabilities are associated with electromagnetic field fluctuations.

The fundamental statistical properties of electric field fluctuation are obtained from the traditional analysis using the Fast Fourier Transformation (FFT). Figure 1 shows the spectrum of electric field fluctuation at $\rho \sim 0.35$, with coherence between electric field fluctuations at two toroidal positions. The spectrum can be divided into four ranges, i) a lower frequency range less than $f < 1.5$ kHz with a quite high coherence of ~ 0.7 , ii) an inertia range of $f < 10$ kHz, iii) the range of $10 < f < 30$ kHz with a sharp

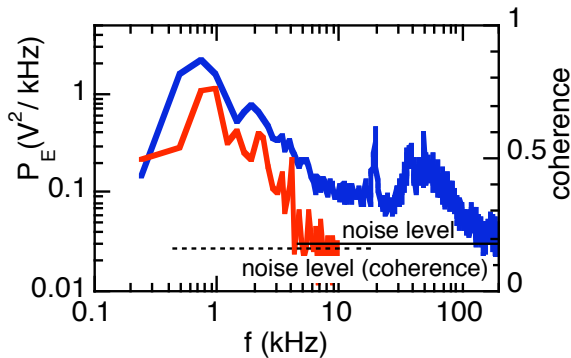


Fig. 1 A spectrum of electric field fluctuation. The measurement is carried out at $\rho \sim 0.35$ (solid line). The coherence between electric field fluctuations at two toroidal locations (dashed line). The coherence is plotted in the low frequency range where the result is above the noise level (in ref. [22])

peak, and iv) the background turbulence range with a broad-band peak around ~ 50 kHz. The fluctuation in $f \sim 2$ kHz to show a long-distance correlation is regarded as the zonal flow. Besides the sharp peak at 19 kHz, there can be seen the other two peaks (at least) at 38 and 57 kHz. These three modes have a long-distance characteristic, since the coherence between the potential fluctuation and that of electric field at the other toroidal position gives a quite high value for three peaks (>0.5). Therefore, the peaks are conjectured as the GAMs. The detailed analysis of the coherent modes is available in ref. [18].

The intermittent characteristics of fluctuation can be extracted using a wavelet analysis. Figure 2a shows an example of the evolution of the zonal flow $Z(t)$ and the wavelet power spectrum of electric field fluctuation $W(f,t)$ at $\rho \sim 0.35$. The used wavelet analysis [27] has the natural correspondence with the traditional Fourier transformation. The zonal flow component is filtered out from electric field fluctuation using a numerical low-pass filter (see details in ref. [7]). Note that the positive value means the ion diamagnetic direction. The zonal flow amplitude (the blue dashed line) shows a slow change in confinement time scale.

Figure 2b shows three plots of normalized fluctuation power as a function of the normalized zonal

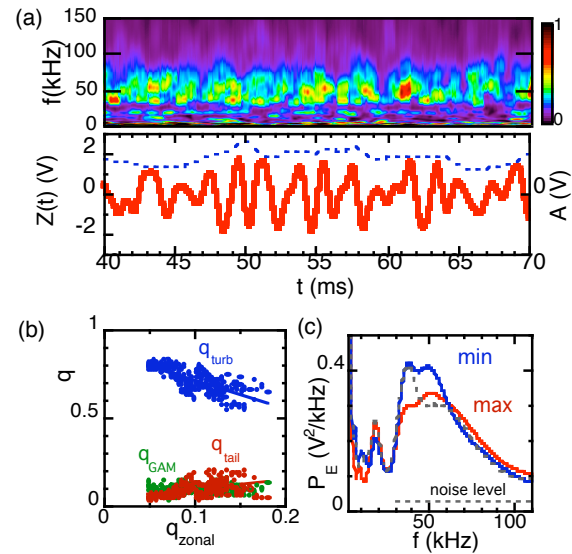


Fig. 2 (a) Evolutions of wavelet spectrum of electric field fluctuations as a function of frequency, and evolution of zonal flow with low-pass filtered. The unit of the color bar is in V^2/kHz . (b) Fluctuation power fractions in three frequency regimes as a function of zonal flow power fraction. (c) Conditional averaged spectra of wavelet power in the local maxima and minima of the zonal flow. The grey dashed line represents the conditional averaged spectrum when $|Z(t)| \sim 0$ (in ref. [22])

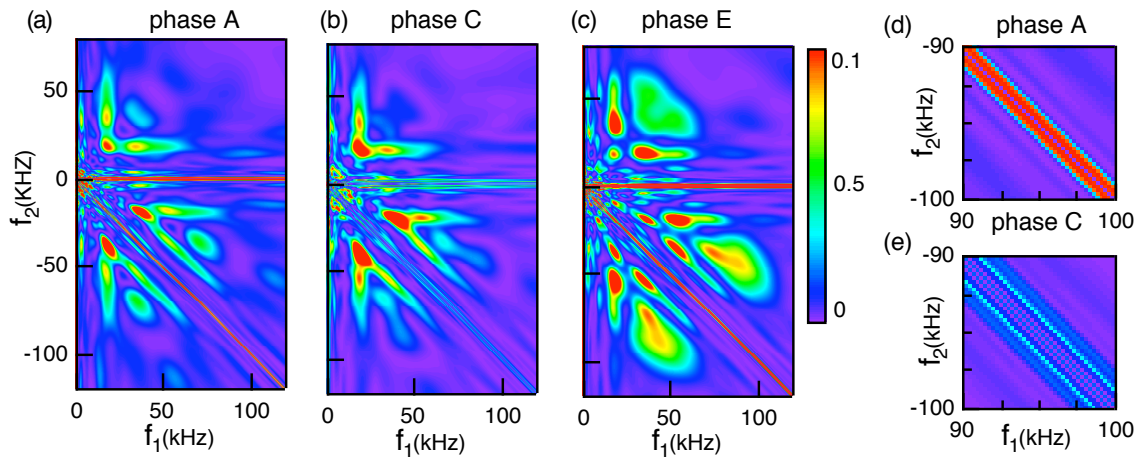


Fig. 3 Diagrams of wavelet squared bicoherence for three phases of zonal flow. The zonal flow is divided into five phases in its magnitude as is shown in Fig. 2a for the conditional integral of the wavelet bicoherence. (a) Bicoherence diagram of the phase A (maximum), (b) that of the phase C (zero) and (c) that of the phase E (minimum). (d) An expanded view of the diagram for the phase A, and (e) another for the phase C [in ref. [23]].

flow power, $q_{zonal}(=q(0.25,1.5 \text{ kHz}))$. The regression analysis shows that the turbulence power $q_{turb}(30,200)$ should be strongly dependent on the zonal flow power as $q_{turb} \sim 0.9-1.6 q_{zonal}$ with their correlation coefficient being $\gamma=0.74$, while no significant relation $\gamma=-0.01$ is found for the fluctuation power of the coherent mode $q_{GAM}(10,30)$. On the other hand, the fluctuation neighboring to the zonal flow shows a positive correlation ($\gamma=0.49$), and follows the zonal flow concomitantly like a tail as $q_{tail}(1.5,10) \sim 0.63 q_{zonal}$. Accordingly, the zonal flow power fraction increases as the turbulence power fraction decreases [22].

In comparison between zonal flow and the wavelet fluctuation powers (Fig. 2a), the colored pattern seems to be synchronous with the tide of the zonal flow. The phase dependency can be examined by taking the conditional averages of the wavelet spectra for the phase of zonal flow. Figure 2c shows the conditional averaged wavelet spectra for the maxima and minima of the zonal flow. It is obvious that the fluctuation power around $\sim 50 \text{ kHz}$ shows an increase (an decrease) around a local minimum (a maximum) of the zonal flow. In addition, the FFT analysis indicates that the modulation frequency of $W(f,t)$ all over the frequencies should coincide with the zonal flow frequency. The result suggests that the fluctuation characteristics should be varied with the phase of zonal flow, as well as with its amplitude [22].

The wavelet bicoherence analysis [27] could be useful in order to reveal the *hidden* linkage between the zonal flow and fluctuations. The analysis is extended to adopt a conditional average in consideration for the

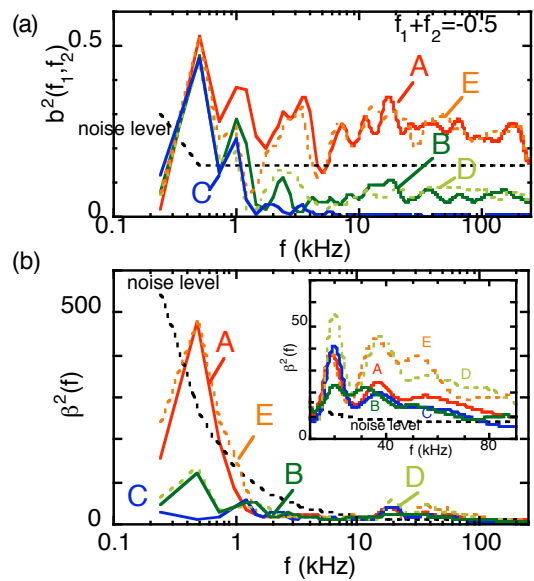


Fig. 4 (a) The squared bicoherence along the line of $f_1+f_2=-0.5 \text{ kHz}$ for the five phases of the zonal flow. (b) Summed squared bicoherence for the five phases of the zonal flow. The green and red solid (dashed) lines represent the zonal flow phases of A and B (E and D), respectively. The blue solid line indicates the phase C. The inset is an expanded view of the frequency range from 10 kHz to 90 kHz (in ref. [23]).

dependency of the fluctuations on the zonal flow phase [23]. The conditional bicoherence is evaluated on the electric field fluctuation for five phases of the zonal flow

(see Fig. 2b); A) $Z(\tau) > 0.8$ V, B) $0.8 > Z(\tau) > 0.25$ V, C) $0.25 > Z(\tau) > -0.25$ V, D) $-0.25 > Z(\tau) > -0.8$ V, and E) $Z(\tau) < -0.8$ V. The number of used ensembles is approximately the same as ~ 20000 for every case.

Figure 3 shows three bicoherence diagrams for the phases, A, C and E. The results indicate clear changes in the coupling between waves according to the phase of the zonal flow. The most important feature is that the couplings become stronger along the lines of $f_1 + f_2 \sim 0.5, -0.5$ kHz at the phases A (maximum) or E (minimum). The expanded views of a region ($90 < |f| < 100$ kHz) clearly demonstrate that the couplings on the lines of $f_1 + f_2 \sim 0.5$ and -0.5 kHz becomes stronger in the phase A. Figure 4a shows the squared bicoherence as a function of f_1 along the line of $f_1 + f_2 = -0.5$ kHz for every phase of the zonal flow. Obviously, the coupling becomes stronger in the range of $f > 2$ kHz as the absolute value of the zonal flow $|Z(t)|$ increases. However, the coupling of the lower frequency of $f < 2$ kHz is rather high and almost the same for every phase.

As a consequence of degraded independency of ensembles in lower frequency, the statistical noise level of the wavelet bicoherence analysis is usually evaluated according to ref. [27]. The noise level is regarded as, however, a statistically sufficient condition to show the significance of couplings, since the phase of the zonal flow lying in the frequency around $f_3 \sim 0.5$ kHz is conditioned for the evaluation. This finding supports the image that the waves with adjacent frequencies interacts collectively with each other to produce the zonal flow through the processes of such as the modulational instabilities.

The results confirm that the coupling becomes stronger when the zonal flow increases in the absolute value. In two phases, A and E, the level of the summed bicoherence in the frequency range of the zonal flow ($f < 1$ kHz) is significantly large to surpass the maximum noise level, or a statistically sufficient condition for the existence of the coupling. As for the couplings between turbulent waves, as is shown in the inset of Fig. 4b, the total bicoherence in the range of $f > 30$ kHz is larger as the zonal flow is in the opposite direction to the bulk flow. The couplings between turbulent waves are varied with the sign of the zonal flow to cause the modulation of the turbulence power spectrum (Fig. 2c). The corresponding increase in the bicoherence can be seen particularly in the regions around $(f_1, f_2) \sim (50, -80)$ kHz, and $(f_1, f_2) \sim (80, -50)$ kHz in the bicoherence diagram of the phase E (Fig. 3c).

4. Identification of Zonal Magnetic Field

As is similar to the previous case, the target plasma is also produced with electron cyclotron resonance heating of ~ 200 kW, to avoid a large-scale plasma motion

caused by magnetohydrodynamic (MHD) instabilities that interfere with the generation of magnetic fields in the meso-scale range. The plasma parameters in the experiment are; magnetic field strength $B = 0.88$ T and density $n_e \sim 5 \times 10^{12} \text{ cm}^{-3}$. The normalized plasma pressure, β -value, is $\sim 0.2\%$.

Collisionless (or electron) and collisional skin depths are estimated as 2.4 mm and 12 mm at 0.5 kHz, respectively. The magnetic Prandtl number is evaluated as $\mu\nu/\eta \sim 10^2$ using the experimental viscosity of $\nu \sim \chi \sim 10$

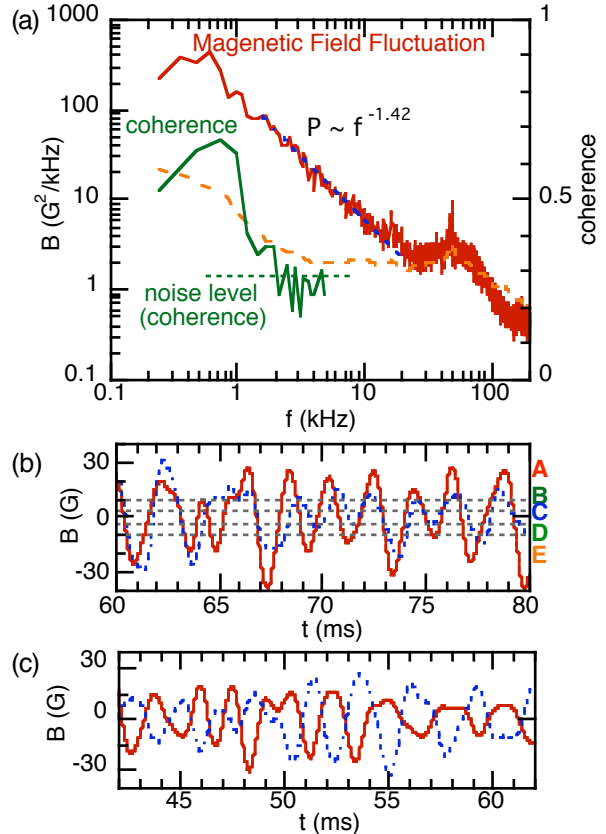


Fig. 5 Magnetic field fluctuation spectrum and existence of mean field. (a) Power spectrum (poloidal component), and coherence between the magnetic field at two toroidal locations. The fluctuation less than ~ 1 kHz shows a quite high coherence, which means generation of global magnetic field of azimuthal symmetry. The spectrum is calculated for the stationary period of ~ 50 ms for the discharge duration of ~ 100 ms with frequency resolution of 0.24 kHz and the Nyquist frequency of 250 kHz. (b) The waveforms of zonal fields at the same radial but different toroidal locations. The positive sign means the direction of vacuum field direction. (c) The other waveforms of zonal fields at the different positions in both toroidal and radial directions. The difference in radial direction is 1 cm (in ref. [25])

m^2/s and resistivity of $\eta \sim 10^{-7} \Omega m$, where χ represents the thermal diffusivity evaluated as the global average from the confinement time.

The measurement was done at the radial position of $r_{obs} = 12 \pm 0.5$ cm, where the signal-to-noise ratio is maximal for the HIBP measurement. In this measurement, it is known from a trajectory calculation that the horizontal beam movement reflects the poloidal magnetic field. A spectrum of the magnetic field fluctuation is shown in Fig. 4, with coherence between two toroidal locations. In the low frequency range, the contamination is sufficiently small, while the electric field contamination may be dominant around ~ 50 kHz and above. The coherence of the frequency lower than 1 kHz is quite high (~ 0.7), which is an average of ~ 70 temporal windows from identical shots; a higher coherence value is obtained in an appropriate period of a single shot. This means that the probing beams are coherently swung by the magnetic field at two toroidal positions. It is unambiguously demonstrated that a mean magnetic field fluctuation with long-distance correlation does exist.

The magnetic field fluctuations in that frequency range are visualized using a low-pass filter [7,22]. Figures 5b and 5c demonstrate two examples of evolution of the magnetic field fluctuation in the frequency range (0.3 - 1 kHz). The zonal field amplitude is evaluated to be ~ 30 G at maximum. The accuracy of the absolute magnetic field value is about 50% owing to uncertainty in the absolute measurement of beam location, although the relative motion of the beam is more precisely measured with accuracy of $\sim 0.1\%$. The in-phase movement of two beams on the same magnetic flux surface (Fig. 5b) suggests that the fluctuation is symmetric or homogeneous around the magnetic axis under the assumption of poloidal symmetry. In contrast, the other waveforms in anti-phase behavior (Fig. 5c), when the position is different in radial direction by 1 cm from the other, suggests that the fluctuation should have a finite radial structure.

A constant phase relation between the signals from two different radial positions, as is shown in Figs 5b and 5c, allows us to estimate the spatio-temporal characteristics of the mean zonal field in the radial direction by calculating the correlation function of low pass-filtered magnetic field fluctuations with spatio-temporal separation of $\Delta r = r' - r$ and $\Delta t = t' - t$. Figure 6a shows the cross-correlation obtained by altering an observed position r' , shot by shot with fixing the other at $r (=12$ cm). Figure 6b illustrates the spatial structure of three times at $\Delta t = 0, 1$ and 2 ms. These correlation diagrams show a quasi-sinusoidal structure in the radial direction with a characteristic radial wavelength of $\lambda_r \sim 1$ cm, while memory of the structure is lost in ~ 2 ms.

These observations in Figs. 5 and 6 show, therefore, the existence of the mean magnetic field with radially zonal structure symmetric around the magnetic axis. This magnetic field resistively damps away, if there is no driving source, on a time scale of $\tau_R = \mu_0 \eta^{-1} k_r^{-2} \sim 50 \mu s$. It cannot be sustained by the external circuit through inductive coupling, because the direction changes with

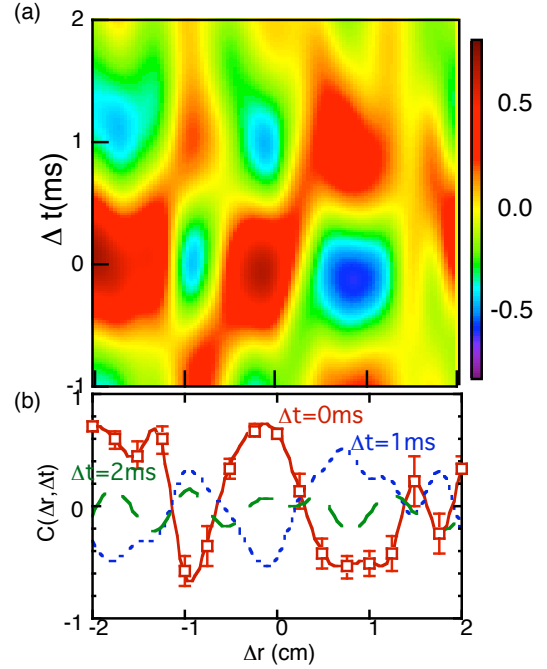


Fig. 6 Radial structure of zonal field. (a) Correlation function of space and time, $C(\Delta r, \Delta t)$, around the radial position of $r=12$ cm. (b) Correlation functions with three different time delays; $\Delta t=0, 1$ and 2 ms. These correlation diagrams show radial structure of zonal field, which has a quasi-sinusoidal radial structure with a characteristic radial wavelength (~ 1 cm) in mesoscale. On the other hand, the temporal correlation indicates that the memory of the mesoscale structure fades away with oscillation in ~ 2 ms (in ref. [25])

radius. It therefore must be sustained by the internal plasma dynamics.

The wavelet bicoherence analysis is applied, as is similar to the case of zonal flow, to quantify the nonlinear coupling strength between the zonal magnetic field and turbulence. The results showed the intermittent coupling between the zonal field and the background turbulence [25]. In this analysis, the contamination of electric field fluctuation in the turbulence regime may disturb the absolute quantification of the coupling between the zonal field and the pure magnetic field turbulence. In the previous measurement [7], the electrostatic mode conjectured as Geodesic Acoustic Mode (GAM) was clearly identified as a sharp peak at ~ 20 kHz in the

electric field spectrum. However, the corresponding peak is completely absent in the magnetic field spectrum. This means that the electric field contamination can be much smaller than the level of the upper boundary shown in Fig. 5. The degree of the contamination could be evaluated more precisely in a future analysis with taking into account the detailed fluctuation properties.

Finally, the presented observations verify the existence of zonal magnetic field, as well as zonal flow, generated from the turbulence, probably through modulational instabilities. From the analogy to the zonal flows in the Jupiter, future observations might find zonal magnetic field structure in a rotating star. A residual macroscopic field could be expected even in the average over the whole zonal structure, in an inhomogeneous background. In addition, the zonal field could serve as a *seed* leading to global instabilities to cause a macroscopic field or dynamo. Therefore, the discovery could be a step toward general understanding the dynamo problem, stimulating a question if the mesoscopic zonal field can be developed into macroscopic structure.

5. Summary

In summary, we have shown two recent findings for turbulence and mesoscale structure, *i.e.*, zonal flow and zonal field. The first one is the direct measurement on electric field fluctuation combined with the wavelet bicoherence analysis, which succeeds to find an intermittent coupling structure between fluctuations, *e.g.*, the zonal flow and turbulence, turbulence and turbulence and so on. The most important finding is that the nonlinear coupling between turbulence changes according to the phase of the zonal flow. The couplings of fluctuations and turbulence to the zonal flow turn visible in the maximum or minimum phases of the zonal flows.

Finally, the presented observations verify the existence of zonal magnetic field, as well as zonal flow, generated from the turbulence, probably through modulational instabilities. A residual macroscopic field could be expected even in the average over the whole zonal structure, in an inhomogeneous background. In addition, the zonal field could serve as a *seed* leading to global instabilities to cause a neoclassical tearing mode in toroidal plasmas, or macroscopic field or dynamo in the universe. Therefore, the discovery could be a step toward general understanding the dynamo problem, stimulating a question if the mesoscopic zonal field can be developed into macroscopic structure.

Acknowledgments

The author thanks Profs. S. Okamura, K. Matsuoka and the members of CHS experimental group for their

cooperation in the experiments, Profs K. Itoh, S-I. Itoh, O. Motojima for their continuous supports. This work is partly supported by the Grant-in-Aids for Specially-Promoted Research (16002005) and Scientific Research (18360447).

References

- [1] G. P. Williams, J. Atom. Sci. **35** 1399 (1978).
- [2] A. Hasegawa, C. G. MacLennan, Y. Kodama, Phys. Fluids **22** 2122 (1979).
- [3] P. H. Diamond, K. Itoh, S-I. Itoh, T. S. Hahm, Plasma Phys. Control. Fusion **47** R35 (2005).
- [4] A. Hasegawa, M. Wakatani, Phys. Rev. Lett. **59** 1581 (1987).
- [5] M. N. Rosenbluth, F. L. Hinton, Phys. Rev. Lett. **80** 724 (1998).
- [6] A. M. Dimits, G. Bateman, M. A. Beer et al., Phys. Plasmas **7** 969 (2000).
- [7] A. Fujisawa et al., Phys. Rev. Lett. **93** 165002 (2004).
- [8] G. R. Tynan, C Holland, J H Yu, A James, D Nishijima, M Shimada and N Taheri, Plasma Phys. Control. Fusion **48** S51 (2006).
- [9] G. S. Xu, B. N. Wan, M. Song, J. Li, Phys. Rev. Lett. **91** 125001 (2003).
- [10] D. K. Gupta, R. J. Fonck, G. R. McKee, D. J. Schlossberg, M. W. Shafer, Phys. Rev. Lett. **97** 125002 (2006).
- [11] M. Jakubowski, R. J. Fonck, G. R. McKee, Phys. Rev. Lett. **89** 265003 (2002).
- [12] M. G. Shats et al., Phys. Rev. Lett. **88** 45001 (2002).
- [13] Y. Hamada et al., Nucl. Fusion **45** 81 (2005).
- [14] T. Ido et al., Nucl. Fusion **46** 512 (2006).
- [15] G. R. McKee et al., Plasma Phys. Control. Fusion **45** A477 (2003).
- [16] G. D. Conway et al., Plasma Phys. Control. Fusion **47** 1165 (2005).
- [17] P. M. Schoch et al., Rev. Sci. Instrum. **74** 1846 (2003).
- [18] A. Fujisawa et al., Plasma Phys. Control. Fusion **48** S31 (2006).
- [19] A. Kramer-Flecken, S. Soldatov, H. R. Koslowski, O. Zimmermann, TEXTOR team, Phys. Rev. Lett. **97** 045006 (2006).
- [20] A. Fujisawa et al., Nucl. Fusion **47** S718 (2007).
- [21] A. Fujisawa et al., Plasma Phys. Control. Fusion **48** S205 (2006).
- [22] A. Fujisawa et al., J. Phys. Soc. Jpn. **76** 033501 (2007).
- [23] A. Fujisawa et al., Plasma Phys. Control. Fusion **49** 211 (2007).
- [24] A. Fujisawa, A. Shimizu, H. Nakano, S. Ohshima, Plasma Phys. Control. Fusion **49** 845 (2007).
- [25] A. Fujisawa et al., Phys. Rev. Lett. **98** 165001 (2007).
- [26] T. P. Crowley, P. M. Schoch, J. W. Heard, R. L. Hickok, X. Y. Yang, Nucl. Fusion **32** 1295 (1992).
- [27] B. Ph. Van Milligen, C. Hidalgo, E. Sanchez, Phys. Rev. Lett. **74** 395 (1995).